An electron paramagnetic resonance study on Sm^{3+} and Yb^{3+} in KY_3F_{10} crystals

2000 J. Phys.: Condens. Matter 12 8727

(http://iopscience.iop.org/0953-8984/12/40/314)

J. Phys.: Condens. Matter **12** (2000) 8727–8736. Printed in the UK PII: S0953-8984(00)14791-5

An electron paramagnetic resonance study on Sm^{3+} and Yb^{3+} in KY_3F_{10} crystals

M Yamaga†, M Honda‡, J-P R Wells§, T P J Han‖ and H G Gallagher‖

† Department of Electrical and Electronic Engineering, Faculty of Engineering, Gifu University, Gifu 501-1193, Japan

‡ Faculty of Science, Naruto University of Education, Naruto, Tokushima 772-8502, Japan

§ FELIX Free Electron Laser Facility, FOM-Institute for Plasma Physics, Rijnhuizen, Edisonbaan 14, 3430 BE Nieuwegein, The Netherlands

‖ Department of Physics and Applied Physics, University of Strathclyde, Glasgow G1 1XN, UK

Received 16 June 2000, in final form 4 August 2000

Abstract. Electron paramagnetic resonance (EPR) spectra of Sm^{3+} and Yb^{3+} ions in KY_3F_{10} single crystals have been measured at X-band microwave frequencies and low temperatures. The EPR lines have been fitted to a tetragonal spin Hamiltonian to determine effective g-values ($g_\parallel$, $g_\perp$). The observed g-values, ($g_\parallel = 0.714(2)$, $g_\perp = 0.11(1)$), for Sm^{3+} are in agreement with those calculated via crystal-field J-mixing of the first excited-state multiplet $^6H_{7/2}$ into the groundstate multiplet $^6H_{5/2}$ of Sm^{3+} as the second-order perturbation. On the other hand, the observed g-values, ($g_\parallel = 5.363(5)$, $g_\perp = 1.306(2)$) for Yb^{3+} are coincident with those calculated via mixing in only the groundstate multiplet $^2F_{7/2}$ as the first-order perturbation because the first excited-state multiplet $^2F_{5/2}$ lies above $\sim$10 000 cm^{-1} from the groundstate. The groundstate eigenfunctions of Sm^{3+} and Yb^{3+} obtained from the EPR results are close to those calculated from a C_{4v} symmetry crystal-field analysis applied to their optical transitions. The distortions of the Sm^{3+} and Yb^{3+} complexes in KY_3F_{10} are discussed in the term of the crystal-field Hamiltonian in comparison with $LiYF_4$.

1. Introduction

Crystals that offer isovalent substitution for trivalent rare-earth ions have received much attention in the literature. Crystals of the $KF–YF_3$ system are a popular choice for their wide transparency, high optical damage threshold and rigid thermomechanical properties [1].

Trivalent rare-earth ions substitute for Y^{3+} ions in KY_3F_{10} and thus reside on a site of C_{4v} point group symmetry. Previous studies of Er^{3+} and Eu^{3+} in KY_3F_{10} confirmed the symmetry of the optically active centre and have established accurate crystal-field and Judd–Ofelt parameters for the ions [2–5]. Indeed KY_3F_{10}:Yb^{3+} has been evaluated for application as an all solid state laser [6]. Previous electron paramagnetic resonance (EPR) studies on KY_3F_{10}:Ho^{3+} [7, 8] revealed a spectacular groundstate hyperfine pattern due to pseudo-quadrupole hyperfine interactions between close lying (5.8 cm^{-1}) groundstate singlets. This is not unlike the situation in CaF_2:Ho^{3+} [9]. Divalent europium has also been observed in KY_3F_{10} [10].

In a previous paper [11], we reported a laser selective site excitation study of KY_3F_{10}:Sm^{3+}/Sm^{2+}. Three Sm^{2+} centres have been identified, being related strongly to significant F^- vacancies near Sm^{2+}. Laser excitation and fluorescence spectroscopy of the single Sm^{3+} centre have revealed 46 energy levels of this centre, being fitted to those calculated by a single electron crystal-field analysis with an assumption that this centre has C_{4v} symmetry. Evidence for fluorine vacancies in KY_3F_{10} has also been observed from measurements of

0953-8984/00/408727+10$30.00

electrical conductivity and dielectric response [12,13], where the dielectric response was found to contain contributions from charge carriers.

In this paper, we report the EPR of Sm^{3+} and Yb^{3+} in KY_3F_{10} at cryogenic temperatures. EPR experiments explore the point group symmetry of the Sm^{3+} and Yb^{3+} centres in the crystals and allow the determination of the eigenfunctions and magnetic properties of the groundstate of these ions. We contrast these studies against those of Sm^{3+} and Yb^{3+} ions in the more well known laser host $LiYF_4$.

2. Experimental details

KY_3F_{10} crystals doped with Sm and Yb ions were grown by the Bridgman–Stockbarger technique [11]. YF_3 and KF were mixed together in essentially stoichiometric amounts taking into account the small amounts (0.01–0.1 mol%) of SmF_3 or YbF_3 to be added. A slight positive pressure of purified argon gas was employed as the growth atmosphere. KY_3F_{10} is a cubic compound with space group O_h^5 ($Fm3m$). The complex is composed of a central Y^{3+} ion sandwiched between two parallel planes, which each contain four F^- ligand ions. One of the planes is rotated 45° perpendicular to the crystal axis, for example, the *c*-axis. There are two other equivalent complexes in the crystal, that is, the rotation axis is parallel to the *a*- and *b*-axes.

EPR measurements were made with a Bruker EMX10/12 X-band spectrometer with microwave frequencies ($\simeq$9.69 GHz), a microwave power of 0.01 mW, and 100 kHz magnetic field modulation. Temperatures in the range of 5–300 K were controlled by continuous-gas-flow and a heater in the cryostat. The angular variation of the EPR spectra was measured by rotating a sample within the cavity. The full range of the applied magnetic fields during an experiment was 0–1.5 T.

3. Experimental results

Sm^{3+} and Yb^{3+} ions have the $4f^5$ and $4f^{13}$ electronic configurations, where the groundstate multiplets are represented by $^6H_{5/2}$ and $^2F_{7/2}$. The six-fold and eight-fold degenerate states are split into three and four Kramers doublets, respectively, by the electrostatic potential provided by the surrounding ligands. The crystal-field splitting determined by the exact magnitude and symmetry of the crystal-field potential is much larger than the Zeeman splitting relative to the X-band microwave frequency energy ($\sim$0.3 cm^{-1}). Thus, the spin eigenfunction of the groundstate is represented effectively by $|\pm\frac{1}{2}\rangle$, with the result that an EPR resonance line is expected to be a single line in the absence of the fine structure. As there are isotopes of Sm and Yb with the non-zero nuclear spins I, the single line is split into $2I + 1$ lines due to the hyperfine interaction.

Figure 1(a) shows the EPR spectrum of Sm^{3+} in KY_3F_{10} observed at 10 K, with $B \parallel [001]$, and at a microwave frequency of 9.693 24 GHz in comparison with that in $LiYF_4$ [14]. As EPR signals due to unknown impurities were observed, the spectrum is cut at the magnetic field of below 0.85 T. The hyperfine structure due to the ^{147}Sm and ^{149}Sm isotopes with the same nuclear spin $I = \frac{7}{2}$ and natural abundance 15.1% and 13.8%, respectively, should be observable as shown in the lower part of figure 1(a) [14]. However, it could not be observed in KY_3F_{10}:Sm^{3+} due to the low signal-to-noise (S/N) ratio. It was found that two weak EPR signals superimposed upon the intense lines were observed. The separation ($\sim$10 mT) is much smaller than those (60–70 mT, 70–90 mT) between the adjacent hyperfine lines due to the ^{149}Sm and ^{147}Sm isotopes in $LiYF_4$ [14]. Figure 1(b) shows the EPR spectra of Sm^{3+} in KY_3F_{10} with

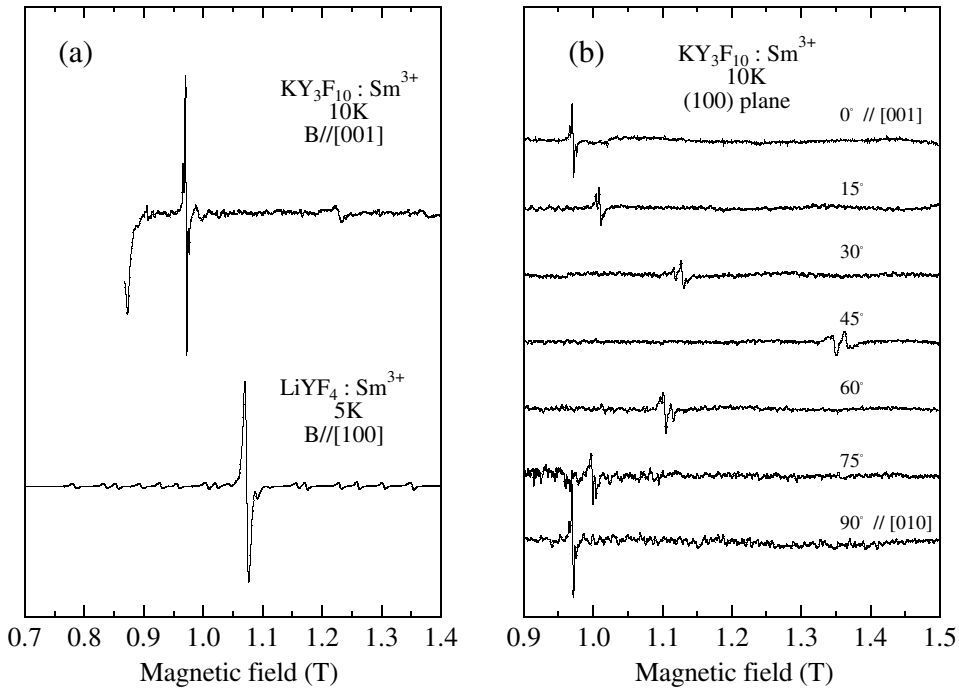

Figure 1. (a) The EPR spectrum of Sm^{3+} in KY_3F_{10} measured at 10 K, with $B \parallel [001]$, and at a microwave frequency of 9.6932 GHz in comparison with that in $LiYF_4$. (b) The angular variation of the EPR spectra of Sm^{3+} in KY_3F_{10} measured with the magnetic field applied in the (100)-plane at 10 K and at microwave frequencies of 9.691–9.693 GHz.

the magnetic field applied in the (100) plane. The spectra with the angles of 30° and 60° between the *c*-axis and the magnetic field show slight shifts of the weak lines from the main line, whereas the 45° spectrum consists of two lines with equal intensities due to magnetically inequivalent Sm^{3+} centres as shown in figure 3(a) later. Therefore, the weak lines are not a part of the hyperfine structure of Sm, but may be due to Sm^{3+} ions perturbed by a nearest-neighbour F^--ion vacancy. Although no evidence for minor centres could be found from exhaustive laser selective excitation studies [11], this must be regarded as a preliminary explanation.

The EPR spectra of Yb^{3+} in KY_3F_{10} measured at low and high magnetic fields with $B \parallel [001]$, at a crystal temperature of 5 K and at a microwave frequency of 9.6927 GHz are shown in figure 2. These can be seen to be composed of an intense central line and several weak lines. The weak lines show two-lines and six-lines hyperfine structures due to the ^{171}Yb and ^{173}Yb isotopes with non-zero nuclear spins of $I = \frac{1}{2}$ and $\frac{5}{2}$, respectively. The relative intensity ratios of the single central line, doublet and sextet are close to those expected from natural abundance 14.3% and 16.1% of the ^{171}Yb and ^{173}Yb isotopes. The central fields of the hyperfine structures due to the ^{171}Yb and ^{173}Yb isotopes are slightly shifted from the intense resonance field to low field and the separation between each adjacent hyperfine line increases as the resonance field increases. This effect can be explained by the second-order perturbation of the hyperfine interaction [14, 15]. The hyperfine parameters estimated from these EPR spectra in figure 2 are summarized in table 1.

The orientational dependences of the positions of the resonance lines of Sm^{3+} and Yb^{3+} for magnetic field rotations in the (100) and (110) planes are plotted in figures 3 and 4,

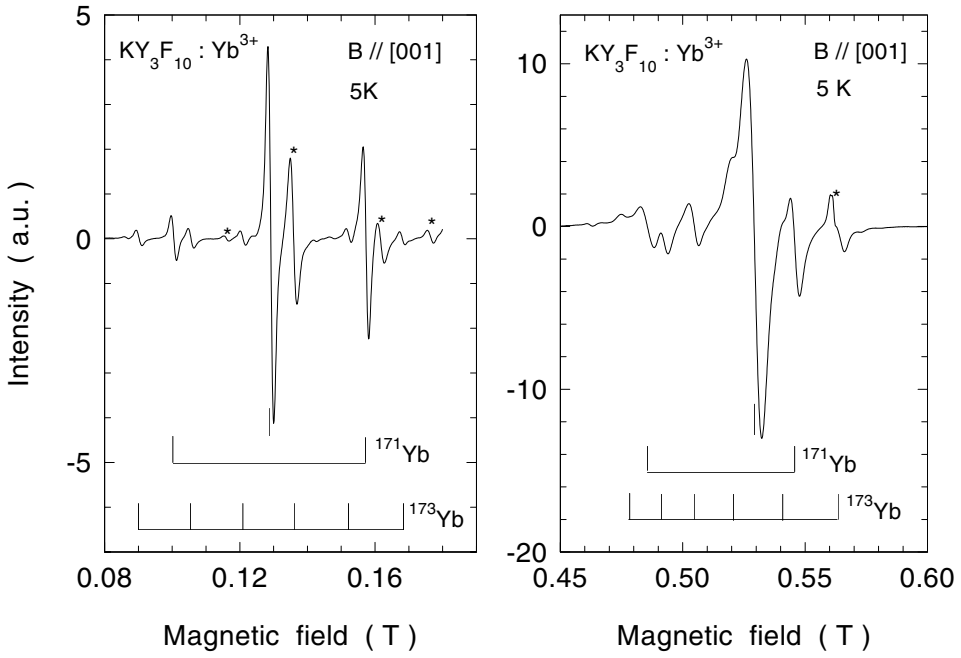

Figure 2. The EPR spectra of Yb^{3+} in KY_3F_{10} measured at low and high magnetic fields with $B \parallel [001]$, a crystal temperature of 5 K and a microwave frequency of 9.6927 GHz. $*$ denotes EPR signals due to unknown impurities. The lines due to hyperfine structure of ^{171}Yb and ^{173}Yb are labelled by the bar diagram below the spectrum.

Table 1. Spin Hamiltonian parameters for Sm^{3+} and Yb^{3+} measured in the KY_3F_{10} crystals in comparison with those in $LiYF_4$.

Crystals	Ion	$g_\parallel$	$g_\perp$	Isotope	$A_\parallel$ (MHz)	$A_\perp$ (MHz)	Ref.
KY_3F_{10}	Sm^{3+}	0.714(2)	0.11(1)	147	—	—	This work
				149	—	—	
	Yb^{3+}	5.363(5)	1.306(2)	171	4280	1100	This work
				173	1170	310	
$LiYF_4$	Sm^{3+}	0.410(5)	0.644(2)	147	205	735	[14]
				149	165	605	
	Yb^{3+}	1.331	3.917	171	1010	3080	[19]
				173	280	850	

respectively. The data are calculated using $h\nu = g\mu_B BS$ where μ_B is the Bohr magneton, B the resonance field, and $S(=\frac{1}{2})$ an effective spin. An effective Hamiltonian appropriate to tetragonal symmetry is given by [15]

$$\mathcal{H} = \mu_B g_\parallel B_z S_z + \mu_B g_\perp (B_x S_x + B_y S_y). \tag{1}$$

The principal z-, x- and y-axes, respectively, of the spectra are the [001], [100] and [010] axes of the crystal. There are three magnetically inequivalent centres in the crystals. Their principal axes are given permitatively by [100], [010] and [001].

Although a part of the angular variation of the Sm^{3+} signals in the (100) plane in figure 3(a) could not be observed because of the small g-values, both variations in the (100) and (110) planes strongly suggest that the Sm^{3+} centre has tetragonal symmetry. The small splitting for

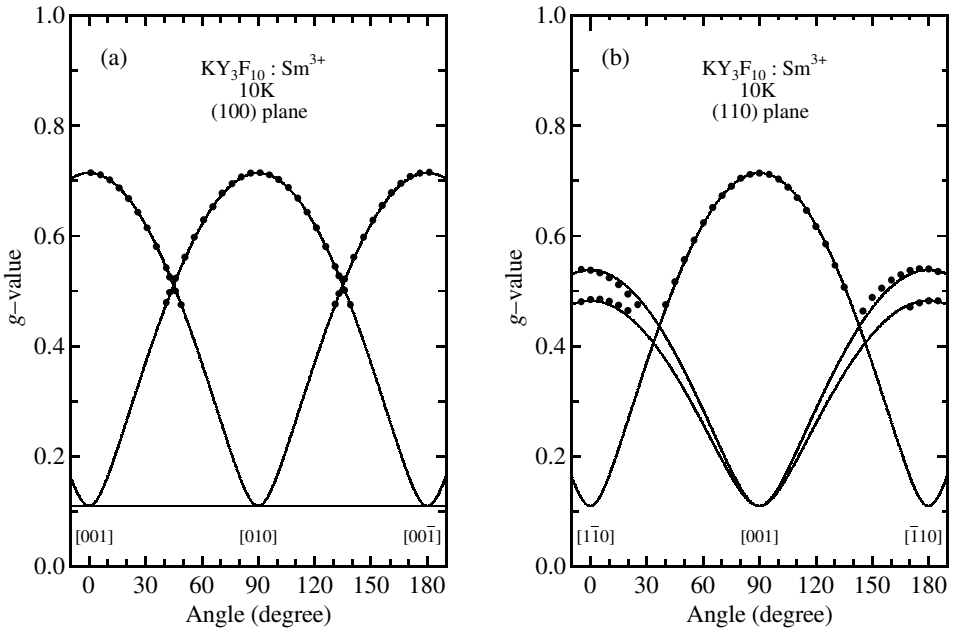

Figure 3. The angular dependence of the resonance lines of Sm^{3+} with the magnetic field applied in: (a) the (100) plane; and (b) the (110) plane. The full curves are calculated using equation (1) and the g-values of Sm^{3+} in table 1. The small splitting of the resonance lines in (b) is due to the misalignment between the crystal axis and magnetic field direction. The full curves in (b) are calculated taking account of the misalignment with the deviation of 3°.

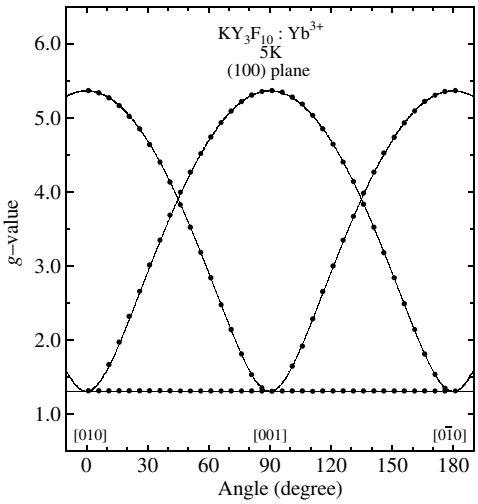

Figure 4. The angular dependence of the intense resonance lines of Yb^{3+} ($I = 0$) with the magnetic field applied in the (100) plane. The full curves are calculated using equation (1) and the g-values of Yb^{3+} in table 1.

the (110) plane in figure 3(b) is due to misalignment between the crystal axis and magnetic field direction and the calculation takes account of the misalignment with the deviation of 3°.

The full curves in figure 3 were calculated using equation (1) and the g-values of Sm^{3+} in table 1 and fit well the observed data.

The angular variation of the intense signals of Yb^{3+} in the (100) plane in figure 4 shows a typical tetragonal pattern. The curves in figure 4 calculated using equation (1) and the g-values of Yb^{3+} in table 1 fit well the observed data.

4. Discussion

4.1. g-tensor

Sm^{3+} and Yb^{3+} ions substitute for Y^{3+} ions in the KY_3F_{10} crystals and thus reside on a site of C_{4v} symmetry. This fact has been confirmed by the EPR study presented in this work. In the KY_3F_{10} lattice the complex composed of Y^{3+} and eight F^- ligands is axially distorted. The Hamiltonian of the crystal-field potential which has a C_{4v} tetragonal distortion [16] is

$$\mathcal{H}_{cf} = B_0^2 C_0^{(2)} + B_0^4 C_0^{(4)} + B_0^6 C_0^{(6)} + B_4^4 (C_4^{(4)} + C_{-4}^{(4)}) + B_4^6 (C_4^{(6)} + C_{-4}^{(6)}) \qquad (2)$$

where $C_n^{(m)}$ are tensor operators and B_n^m are expansion coefficients of spherical harmonics.

The g-tensors of Sm^{3+} and Yb^{3+} ions are calculated using the eigenfunctions of the respective groundstates $^6H_{5/2}$ and $^2F_{7/2}$ split by the tetragonal distortion. We discuss the g-tensors of the Sm^{3+} and Yb^{3+} in the KY_3F_{10} crystals, separately.

4.1.1. Sm^{3+}. In the case of a strong tetragonal field ($|B_4^4 C_4^{(4)}| \ll |B_0^2 C_0^{(2)}|, |B_0^4 C_0^{(4)}|$), the eigenfunctions of the Hamiltonian for $^6H_{5/2}$ are given by $|J, J_z\rangle = |\frac{5}{2}, \pm\frac{1}{2}\rangle, |\frac{5}{2}, \pm\frac{3}{2}\rangle$, and $|\frac{5}{2}, \pm\frac{5}{2}\rangle$. The operator $C_4^{(4)}$ mixes the spin states $|\frac{5}{2}, \pm\frac{3}{2}\rangle$ and $|\frac{5}{2}, \mp\frac{5}{2}\rangle$. The optical spectra of Sm^{3+} in the KY_3F_{10} crystal indicate that the energy levels of the first excited-state multiplet $^6H_{7/2}$ lie above $\sim$1200 cm^{-1} from the groundstate multiplet $^6H_{5/2}$ [11]. The mixing of $^6H_{7/2}$ into $^6H_{5/2}$ occurs through the second-order perturbation of the operators $C_0^{(m)}$ ($m = 2, 4$) [15, 16]. The normalized eigenfunctions of the three Kramers doublets of the groundstate multiplet $^6H_{5/2}$ are modified through the inclusion of the crystal-field J-mixing to be as

$$|\pm\tilde{\tfrac{1}{2}}\rangle = a_1|\tfrac{5}{2}, \pm\tfrac{1}{2}\rangle \pm p_1|\tfrac{7}{2}, \pm\tfrac{1}{2}\rangle \pm q_1|\tfrac{7}{2}, \mp\tfrac{7}{2}\rangle \qquad (3)$$

$$|\pm\tilde{\tfrac{3}{2}}\rangle = a_2|\tfrac{5}{2}, \pm\tfrac{3}{2}\rangle + b_2|\tfrac{5}{2}, \mp\tfrac{5}{2}\rangle \pm p_2|\tfrac{7}{2}, \pm\tfrac{3}{2}\rangle \pm q_2|\tfrac{7}{2}, \mp\tfrac{5}{2}\rangle \qquad (4)$$

$$|\pm\tilde{\tfrac{5}{2}}\rangle = a_3|\tfrac{5}{2}, \pm\tfrac{5}{2}\rangle + b_3|\tfrac{5}{2}, \mp\tfrac{3}{2}\rangle \pm p_3|\tfrac{7}{2}, \pm\tfrac{5}{2}\rangle \pm q_3|\tfrac{7}{2}, \mp\tfrac{3}{2}\rangle \qquad (5)$$

where a_i, b_i, p_i and q_i ($|p_i|, |q_i| \ll |a_i|, |b_i|$) are mixing parameters and $a_i^2 + b_i^2 + p_i^2 + q_i^2 = 1$.

The g-values for $|\pm\tilde{\frac{1}{2}}\rangle$ are calculated to be

$$g_\parallel = \left|\frac{2}{7}a_1^2 + \frac{52}{63}(p_1^2 - 7q_1^2) + \frac{12\sqrt{10}}{7}a_1 p_1\right| \qquad (6)$$

$$g_\perp = \left|\frac{6}{7}a_1^2 - \frac{208}{63}p_1^2 - \frac{6\sqrt{10}}{7}a_1 p_1\right|. \qquad (7)$$

The g-values for $|\pm\tilde{\frac{3}{2}}\rangle$ are calculated to be

$$g_\parallel = \left|\frac{2}{7}(3a_2^2 - 5b_2^2) + \frac{52}{63}(3p_2^2 - 5q_2^2) + \frac{2}{7}(10\sqrt{3}a_2 p_2 + 6\sqrt{5}b_2 q_2)\right| \qquad (8)$$

$$g_\perp = \left|\frac{2}{7}(2\sqrt{5}a_2 b_2) - \frac{52}{63}(4\sqrt{3}p_2 q_2) + \frac{2}{7}(15a_2 q_2 + \sqrt{15}b_2 p_2)\right|. \qquad (9)$$

The g-values for $|\pm\tilde{\frac{5}{2}}\rangle$ are calculated in the same way as for $|\pm\tilde{\frac{3}{2}}\rangle$.

The pure eigenfunction of $|\frac{5}{2}, \pm\frac{1}{2}\rangle$ gives the g-values ($g_\parallel = \frac{2}{7}, g_\perp = \frac{6}{7}$) which do not fit the observed g-values $g_\parallel = 0.714$, $g_\perp = 0.11$ of KY_3F_{10}:Sm^{3+} in table 1. Although the g-values calculated using equations (6) and (7) and the mixing parameters $a_1 = 0.588$, $p_1 = -0.668$ and $q_1 = 0.457$ are close to the observed g-values, the large values of p_1 and q_1 are inconsistent with the second-order perturbation theory. Next, we apply the g-values to the case of $|\pm\tilde{\frac{3}{2}}\rangle$. In principle it is difficult to determine the four parameters a_2, b_2, p_2, and q_2 in equations (8) and (9) from the two observed g-values and the constraint imposed by wavefunction normalization ($a_2^2 + b_2^2 + p_2^2 + q_2^2 = 1$). We have obtained best fit values for these parameters using a least squares regression technique under the assumption that $|a_2|, |b_2| \gg |p_2|, |q_2|$. The calculation has started from an initial set of $(a_2, b_2, p_2, q_2) = (1, 0, 0, 0)$ or $(0, 1, 0, 0)$. The two sets of g-values are calculated to be ($g_\parallel = 0.71, g_\perp = 0.11$) with $(a_2, b_2, p_2, q_2) = (0.96, 0.27, 0.02, -0.06)$ and ($g_\parallel = 0.73, g_\perp = 0.11$) with $(a_2, b_2, p_2, q_2) = (0.04, 0.97, 0.19, 0.15)$, respectively. These differ in which ket vector represents the dominant component and it is difficult to identify which eigenfunction most closely represents the physical situation in KY_3F_{10} from this data alone.

4.1.2. Yb^{3+}. The $4f^{13}$ configuration appropriate for Yb^{3+} can be represented by a single hole. Thus the splitting of the degenerate configuration by the spin–orbit interaction yields two free-ion LSJ multiplets ($^2F_{7/2}$, $^2F_{5/2}$) split by an energy of $\sim$10 000 cm^{-1}. As a consequence of this we may neglect any mixing of $^2F_{5/2}$ and $^2F_{7/2}$. Therefore the eigenfunctions of $^2F_{7/2}$ [17–19] can be represented as:

$$|\pm\tilde{\tfrac{1}{2}}\rangle = c_1|\tfrac{7}{2}, \pm\tfrac{1}{2}\rangle + d_1|\tfrac{7}{2}, \mp\tfrac{7}{2}\rangle \tag{10}$$

$$|\pm\tilde{\tfrac{3}{2}}\rangle = c_2|\tfrac{7}{2}, \pm\tfrac{3}{2}\rangle + d_2|\tfrac{7}{2}, \mp\tfrac{5}{2}\rangle \tag{11}$$

$$|\pm\tilde{\tfrac{5}{2}}\rangle = c_2|\tfrac{7}{2}, \mp\tfrac{5}{2}\rangle - d_2|\tfrac{7}{2}, \pm\tfrac{3}{2}\rangle \tag{12}$$

$$|\pm\tilde{\tfrac{7}{2}}\rangle = c_1|\tfrac{7}{2}, \mp\tfrac{7}{2}\rangle - d_1|\tfrac{7}{2}, \pm\tfrac{1}{2}\rangle. \tag{13}$$

The g-values for $|\pm\tilde{\frac{1}{2}}\rangle$ are calculated to be

$$g_\parallel = \tfrac{8}{7}|c_1^2 - 7d_1^2| \tag{14}$$

$$g_\perp = \tfrac{32}{7}c_1^2. \tag{15}$$

The g-values for $|\pm\tilde{\frac{3}{2}}\rangle$ are calculated to be

$$g_\parallel = \tfrac{8}{7}|3c_2^2 - 5d_2^2| \tag{16}$$

$$g_\perp = \tfrac{8}{7}|4\sqrt{3}c_2d_2|. \tag{17}$$

The g-values for $|\pm\tilde{\frac{5}{2}}\rangle$ and $|\pm\tilde{\frac{7}{2}}\rangle$ are calculated in the same way as for $|\pm\tilde{\frac{3}{2}}\rangle$ and $|\pm\tilde{\frac{1}{2}}\rangle$, respectively.

The observed g-values of KY_3F_{10}:Yb^{3+} in table 1 are $g_\parallel = 5.363(5)$, $g_\perp = 1.306(2)$. The g-values are calculated to be ($g_\parallel = 5.363, g_\perp = 1.306$) using equations (14) and (15) with $|c_1| = 0.537$, $|d_1| = 0.844$, and ($g_\parallel = 5.446, g_\perp = 1.337$) using equations (16) and (17) with $|c_2| = 0.171$, $|d_2| = 0.985$, respectively, where the signs of the mixing parameters cannot be determined by the g-values. Both calculated values are very close to the observed ones. As with the Sm^{3+} g-values, it is difficult to unambiguously determine which eigenfunction is the most accurate.

The same calculation of the g-values of Yb^{3+} in several scheelite crystals has been done by Sattler and Nemarich [18]. They have concluded that the observed g-values of Yb^{3+} in

the crystals are plotted on the relation curve between $g_\parallel$ and $g_\perp$ calculated for the Kramers doublets $\Gamma_{5,6}$ of $^2F_{7/2}$.

In addition, the experimental ratio of the hyperfine parameters of the ^{171}Yb and ^{173}Yb isotopes in KY_3F_{10}, $^{171}A_\parallel/^{173}A_\parallel = 3.658$, agrees with the ratio of the nuclear magnetic moments $^{171}\mu_\parallel/^{173}\mu_\parallel = -3.638$. The relation of $g_\parallel/g_\perp = A_\parallel/A_\perp$ is derived from the first-order theory [15]. The experimental ratios of $g_\parallel/g_\perp = 4.106$ and $A_\parallel/A_\perp = 3.89$ and 3.77 for ^{171}Yb and ^{173}Yb satisfy approximately the relation. This fact leads us to deduce that the g-values are enough to be calculated by the first-order perturbation.

4.2. Crystal-field calculations

In the previous paper [11], we reported the energy levels of the multiplets of Sm^{3+} obtained from the laser excitation and fluorescence and determined those calculated using a Hamiltonian including the free ion and crystal-field parameters. The dominant components of the eigenfunction of the groundstate, $^6H_{5/2}Z_1\gamma_7$, of Sm^{3+} in KY_3F_{10} [11] is given by,

$$|^6H_{5/2}Z_1\gamma_7\rangle = 0.0617|\tfrac{5}{2}, \pm\tfrac{3}{2}\rangle - 0.9805|\tfrac{5}{2}, \mp\tfrac{5}{2}\rangle \mp 0.0133|\tfrac{7}{2}, \pm\tfrac{3}{2}\rangle \pm 0.1699|\tfrac{7}{2}, \mp\tfrac{5}{2}\rangle. \quad (18)$$

The g-values are calculated to be ($g_\parallel = 2.13$, $g_\perp = 0.135$) using equation (18). The calculated value of $g_\parallel$ is larger than the observed one. However, the g-values are calculated to be ($g_\parallel = 0.87$, $g_\perp = 0.12$) using the complete eigenfunction of the groundstate and in agreement with the observed ones. This suggests that the signs and magnitudes of the mixing coefficients of the higher excited-state multiplets ^6H_J ($J = \frac{7}{2}, \frac{9}{2}, \frac{11}{2}, \frac{13}{2}$) are very sensitive to the magnitude of $g_\parallel$.

The groundstate eigenfunction, $^2F_{7/2}Z_1\gamma_7$, of Yb^{3+} can be calculated using the crystal-field Hamiltonian with the same parameters as Sm^{3+}. The calculated eigenfunction is given by

$$|^2F_{7/2}Z_1\gamma_7\rangle = 0.21|\tfrac{7}{2} \pm \tfrac{3}{2}\rangle + 0.98|\tfrac{7}{2} \mp \tfrac{5}{2}\rangle. \quad (19)$$

The crystal-field calculation supports the choice of $|\pm\tilde{\tfrac{3}{2}}\rangle$ with $|c_2| = 0.171$, $|d_2| = 0.985$ in equation (11). The optical spectra of Yb^{3+} show that the energy levels of the first excited-state multiplet $^2F_{5/2}$ lie above $\sim$10 000 cm^{-1} from the groundstate multiplet $^2F_{7/2}$. The eigenfunctions of Yb^{3+} calculated using a crystal-field Hamiltonian as the first-order perturbation can explain the EPR and optical results.

4.3. Comparison between KY_3F_{10} and $LiYF_4$

In the case of a strong tetragonal field ($|B_4^4C_4^{(4)}| \ll |B_0^2C_0^{(2)}|, |B_0^4C_0^{(4)}|$ in equation (2)), the eigenfunctions for $^6H_{5/2}$ of Sm^{3+} are given by $|J, J_z\rangle = |\frac{5}{2}, \pm\frac{1}{2}\rangle, |\frac{5}{2}, \pm\frac{3}{2}\rangle$, and $|\frac{5}{2}, \pm\frac{5}{2}\rangle$. If the main component of the crystal-field Hamiltonian is assumed to be $B_0^2C_0^{(2)}$, the positive or negative sign of B_0^2 determines that the Kramers doublet, $|J, J_z\rangle$, of the groundstate is $|\frac{5}{2}, \pm\frac{1}{2}\rangle$ or $|\frac{5}{2}, \pm\frac{5}{2}\rangle$, respectively. As the $C_0^{(2)}$ tensor is transformed equivalently as the form of $3J_z^2 - J(J+1)$ [15, 16], the positive or negative sign of B_0^2 is associated with that the electronic density function of the groundstate is expanded or compressed along the z-axis, respectively. In contrast, the $B_4^nC_4^{(n)}$ ($n = 4, 6$) terms which mix the spin states $|\frac{5}{2}, \pm\frac{3}{2}\rangle$ and $|\frac{5}{2}, \mp\frac{5}{2}\rangle$, represent a part of the cubic crystal field.

The C_{4v} crystal-field parameters of B_n^m for KY_3F_{10}:Sm^{3+} [11] and $LiYF_4$:Sm^{3+} [14] are obtained by fitting the experimental energy levels of Sm^{3+} to the calculated energy levels and summarized in table 2. Although the magnitudes of B_0^2 of Sm^{3+} in both crystals in table 2 are about half of those of B_0^4, the contribution of the $B_0^2C_0^{(2)}$ term to the crystal-field splitting of the groundstate multiplet, $^6H_{5/2}$, is larger than that of $B_0^4C_0^{(4)}$. The negative and positive values

Table 2. The C_{4v} crystal-field parameters of KY_3F_{10}:Sm^{3+} and $LiYF_4$:Sm^{3+}. The energy unit is cm^{-1}.

Crystals	B_0^2	B_0^4	B_4^4	B_0^6	B_4^6	Ref.
KY_3F_{10}	−600	−1388	410	596	127	[11]
$LiYF_4$	368	−755	−938	−64	−898	[14]

of B_0^2 for KY_3F_{10} and $LiYF_4$ are obtained in table 2. This is consistent with the EPR results that the dominant component of the Sm^{3+} groundstate, $|\pm\frac{\tilde{3}}{2}\rangle$, in KY_3F_{10} is $|\frac{5}{2}, \pm\frac{5}{2}\rangle$, whereas that in $LiYF_4$ is $|\frac{5}{2}, \pm\frac{1}{2}\rangle$ [14]. The magnitudes of B_4^n ($n = 4, 6$) for $LiYF_4$ in table 2 are larger than those for KY_3F_{10}. The cubic field component for $LiYF_4$ remains more than for KY_3F_{10}.

According to the x-ray structure analysis, the distortion of the complex in KY_3F_{10} is that one of two parallel (001) planes, which each contain four F^- ligand ions, is rotated 45° perpendicular to the [001] axis. On the other hand, the distortion in $LiYF_4$ is such that the four F^- ligand ions located at the cubic corners in each (110) or ($\bar{1}10$) plane move along the [001] axis in directions opposite from each other. These distortions of the complexes show axial symmetry. The groundstate wavefunctions of Sm^{3+} in KY_3F_{10} and $LiYF_4$ which are expected to be expanded in the (001) plane and along the [001] axis, respectively, correspond to the complexes effectively compressed or elongated along the [001] axis.

The crystal-field splitting of Yb^{3+} in the KY_3F_{10} crystals is different from those of Sm^{3+} because of their different eigenfunctions. The contribution of $B_0^4C_0^{(4)}$ to the crystal-field splitting of the groundstate multiplet, $^2F_{7/2}$, of Yb^{3+} is comparable with that of $B_0^2C_0^{(2)}$. The signs and magnitudes of B_0^2 and B_0^4 determine which spin state, $|\frac{7}{2}, J_z\rangle$, of Yb^{3+} is the groundstate. So, it is difficult to discuss the distortions of the Yb^{3+} complexes in KY_3F_{10} and $LiYF_4$ in terms of the crystal-field parameters.

5. Conclusions

We have presented EPR studies of KY_3F_{10} doped with Sm^{2+}/Sm^{3+} and Yb^{3+}. The observed Sm^{3+} EPR spectra are very weak as the majority of samarium ions in the crystal are incorporated in the divalent state due to fluorine vacancies in the host crystal unit cell. From the angular variation of these resonances, we can determine that the point group symmetry at the Sm^{3+} site is tetragonal with mutually orthogonal four-fold axes lying along the [001], [010] and [100] crystallographic directions. We have determined Sm^{3+} groundstate g-values of $g_\parallel = 0.714(2)$ and $g_\perp = 0.11(1)$. The Yb^{3+} EPR spectra with $g_\parallel = 5.363(5)$ and $g_\perp = 1.306(2)$ support also that the symmetry at the Yb^{3+} sites is tetragonal.

The opposite tendency of the g-values and hyperfine-structure parameters of Sm^{3+} and Yb^{3+} in KY_3F_{10} and $LiYF_4$ are strongly associated with the crystal-field potentials expanded as a sum of spherical harmonics. The sign and magnitude of the coefficient of the expanded terms are important to determine the energy levels and eigenfunctions of the rare-earth ions in the crystals.

Acknowledgments

This work has been in a part supported by the Royal Society and the British Council through the award of a joint research project between UK and Japan.

References

[1] Dubinskii M A, Khaidukov N M, Garipov I G, Dem'yanets L N, Naumov A K, Semashko V V and Malyusov V A 1990 *J. Mod. Optics* **37** 1355
[2] Porcher P and Caro P 1976 *J. Chem. Phys.* **65** 89
[3] Porcher P and Caro P 1978 *J. Chem. Phys.* **68** 4176
[4] Porcher P and Caro P 1978 *J. Chem. Phys.* **68** 4183
[5] Heyde K, Binnemans K and GorllerWalrand C 1998 *J. Chem. Soc. Faraday Trans.* **94** 1671
[6] Deloach L D, Payne S A, Chase L L, Smith L K, Kway W L and Krupke W F 1993 *IEEE J. Quant. Electron.* **24** 1179
[7] Malkin B Z, Tarasov V F and Sakurov G S 1995 *JETP Lett.* **62** 811
[8] Tarasov V F, Shakurov G S, Malkin B Z and Hutchinson C A 1997 *J. Alloys Compounds* **250** 364
[9] Martin J P D, Boonyarith T, Manson N B, Mujaji M and Jones G D 1993 *J. Phys.: Condens. Matter* **5** 1333
[10] Joubert M F, Boulon G and Gaume F 1981 *Chem. Phys. Lett.* **80** 367
[11] Wells J-P R, Sugiyama A, Han T P J and Gallagher H G 1999 *J. Lumin.* **85** 91
[12] Toshmatov A D, Aukhadeev F L, Teropilovkiy D N, Dudkin V A, Zhdanov R Sh and Yagudin Sh I 1988 *Sov. Phys.-Solid State* **30** 61
[13] Ayala A P, Oliveira M A S, Gesland J Y and Moreira R L 1998 *J. Phys.: Condens. Matter* **10** 5161
[14] Wells J-P R, Yamaga M, Han T P J, Gallagher H G and Honda M 1999 *Phys. Rev.* B **60** 3849
[15] Abragam A and Bleaney B 1970 *Electron Paramagnetic Resonance of Transition Ions* (Oxford: Clarendon) ch 5 and ch 16
[16] Wybourne B G 1965 *Spectroscopic Properties of Rare Earths* (New York: John Wiley) ch 6
[17] Sattler J P and Nemarich J 1970 *Phys. Rev.* B **1** 4249
[18] Sattler J P and Nemarich J 1970 *Phys. Rev.* B **1** 4256
[19] Sattler J P and Nemarich J 1971 *Phys. Rev.* B **4** 1